



ELSEVIER

Available online at [www.sciencedirect.com](http://www.sciencedirect.com)

 ScienceDirect

Proceedings of the Combustion Institute 31 (2007) 675–683

Proceedings  
of the  
Combustion  
Institute

[www.elsevier.com/locate/proci](http://www.elsevier.com/locate/proci)

## Soot particle size distributions in a well-stirred reactor/plug flow reactor

Samuel L. Manzello<sup>a,\*</sup>, David B. Lenhert<sup>a,1</sup>, Ahmet Yozgatligil<sup>b,c</sup>,  
Michael T. Donovan<sup>b,1</sup>, George W. Mulholland<sup>c</sup>,  
Michael R. Zachariah<sup>b,c</sup>, Wing Tsang<sup>b</sup>

<sup>a</sup> *Building and Fire Research Laboratory, National Institute of Standards and Technology (NIST), Gaithersburg, MD 20899, USA*

<sup>b</sup> *Chemical Science Technology Laboratory, National Institute of Standards and Technology (NIST), Gaithersburg, MD 20899, USA*

<sup>c</sup> *Department of Mechanical Engineering and Chemistry, University of Maryland—College Park, College Park, MD, USA*

### Abstract

A well-stirred reactor (WSR) followed by a plug flow reactor (PFR) is being used to study polycyclic aromatic hydrocarbon (PAH) growth and soot inception. Soot size distributions were measured using a dilution probe followed by a nano-differential mobility analyzer (Nano-DMA). A rapid insertion probe was fabricated to thermophoretically collect particles from the reactor for transmission electron microscopy (TEM) imaging. Results are presented on the effect of equivalence ratio on the soot size distributions obtained for fixed dilution ratio, the effect of dilution ratio on the soot size distributions obtained for fixed equivalence ratio, and the effect of temperature on the soot size distributions obtained for fixed equivalence ratio. In addition to particle sizing measurements, gas samples were analyzed by a gas chromatograph to determine the concentration of gaseous species in the PFR thought to be important in soot formation. Our soot size distribution measurements demonstrate that the mixing conditions in the flame zone affect whether or not a nucleation mode was detected in the size distribution.

Published by Elsevier Inc. on behalf of The Combustion Institute.

*Keywords:* Incipient soot; Nano-DMA; TEM

### 1. Introduction

Release of soot into the atmosphere by combustion processes contributes to environmental

and health hazards. Unfortunately, understanding the mechanisms responsible for soot formation remains a daunting task. The process of soot inception is the least understood aspect of soot formation [1,2].

It has long been recognized that a well-stirred reactor (WSR) coupled with a plug flow reactor (PFR) has many advantages for soot inception studies compared to laminar flames [3]. A WSR/PFR provides combustion conditions that are

\* Corresponding author. Fax: +1 301 975 4052.

E-mail address: [samuel.manzello@nist.gov](mailto:samuel.manzello@nist.gov) (S.L. Manzello).

<sup>1</sup> NRC-NIST Post-Doctoral Fellow.

closer to industrial scale combustors (e.g., gas turbines) when compared to laminar flames. To advance the understanding of soot inception in combustion systems requires detailed measurements of soot particle size distributions under conditions of incipient particle formation. Such measurements are needed to validate models of soot formation in flames. Differences in flame structure, such as mixing, may be important to understand soot formation for practical combustors [1,2].

The goal of this study was to measure soot particle size distributions in a WSR/PFR using a diluter coupled with a nano-differential mobility analyzer (Nano-DMA). A diluter was used to minimize both coagulation growth of the particles and thermophoretic deposition on the sampling tube. The dilution probe described herein allowed for dilution ratios of up to  $10^4$ , which are considerably larger than previously reported measurements in a WSR/PFR [4]. In addition, a rapid insertion probe was fabricated to thermophoretically collect particles from the reactor for transmission electron microscopy (TEM) imaging.

## 2. Experimental description

This study utilized the NIST WSR/PFR to examine soot inception of rich ethylene/air oxidation at atmospheric pressure [5]. The WSR, originally developed in 1955 [6], has been used extensively to study PAH and soot [3]. The NIST WSR reactor was based on the design currently implemented by Stouffer et al. [7]. The WSR consists of a 250 ml toroidal chamber made of an upper and lower section of silicon carbide (SiC). An Inconel jet ring is located between the two SiC sections. The jet ring consists of 48 nozzles (1 mm diameter) which inject the premixed fuel/air mixture at near sonic velocities. The resulting jets of fuel/air mixture cause rapid macroscopic and microscopic mixing of reactants, intermediates, and products within the WSR, approximating a highly turbulent combustion environment.

The air and gaseous fuel flow rates were controlled using Brooks Instruments<sup>2</sup> mass flow controllers. The air system (filtered and dried) was designed to accommodate flow rates up to 400 SLPM with pre-heat temperatures up to 473 K. The fuel system was designed to provide a steady flow of up to 75 SLPM. As a result, the residence times of the WSR can be varied between 5 and 12 ms.

The exhaust gases from the WSR enter the PFR section through a silicon carbide flow

straightener. The PFR section includes an inner Halcis-I (SiC) tube surrounded by an outer alumina insulating sleeve, all of which is encased in a steel vessel. The inner Halcis-I tube is 70 cm long and has an inner diameter of 5.1 cm. Four sampling ports are spaced every 15.2 cm along the length of the reactor. All sampling was performed in the bottom-most port of the PFR section (closest to WSR section). The gas velocity in the PFR section is a function of flow conditions into the WSR; in the present study the velocity is on the order of 10 m/s.

The fuel rich conditions necessary for soot inception resulted in volume fractions of carbon monoxide (CO) in excess of 15% volume (dry). An afterburner was installed after the PFR section to burn out most of the CO (for safety reasons). The products were then cooled using a water spray nozzle prior to being released to ambient.

The dilution probe used during these experiments was based upon the design of Zhao et al. [8]. Figure 1 shows a schematic of the diluter. It is important to recognize that the dilution probe used in the present study was gas-cooled, as opposed to a water cooled dilution probe used by Zhao et al. [8]. It was simpler to use a gas-cooled probe in our WSR/PFR, as it avoids a hazardous condition if water leaked or over-heated and gas cooling provided less thermal gradients. The dilution probe was made from a 400 mm long Inconel 601 tube (6.15 mm OD, 5.15 mm ID) with a single 0.50 mm orifice in the side wall for sampling the particulate and other combustion products. Nitrogen flow through the tube was controlled by a mass flow controller, which was held constant at 30 SLPM. To insulate the Inconel from the reactor stream, two zirconia ceramic sleeves (9.53 mm OD, 6.35 mm ID, 63.5 mm long) were bonded to the Inconel tube starting approximately 2.0 mm from each side of the orifice. The resulting gap was partially covered with a ceramic paste to help reduce the temperature of the Inconel tube. Using this technique resulted in a dilution exhaust temperature of 160 °C. An ejector pump was used to adjust the pressure drop

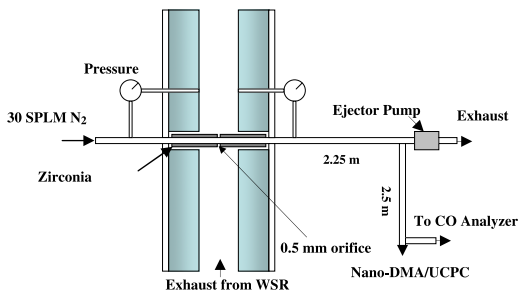


Fig. 1. Dilution probe, installed in the PFR section, coupled to Nano-DMA/UCPC.

<sup>2</sup> Certain commercial equipment is identified in this paper to accurately describe the experimental procedure, this in no way implies endorsement by NIST.

across the orifice to vary the dilution ratio from  $10^2$  to  $10^4$ .

A portion of the diluted flow immediately prior to the ejector pump was directed to a non-dispersive infrared (NDIR) analyzer for CO measurements (Horiba Model VIA-510) and a Nano-DMA/ultrafine condensation particle counter (UCPC) for particle size and concentration measurements. To determine the dilution ratio, a second CO measurement was made of the undiluted PFR stream. The undiluted CO measurement was dried through a combination of wet and dry ice baths. Unlike laminar flame studies, the orifice cannot be cleaned between Nano-DMA scans in the PFR section and small quantities of soot deposits around the orifice can degrade the quality of the size distributions [9]. To mitigate the formation of such growths, the diluter was over pressurized to exhaust nitrogen into the reactor between Nano-DMA scans.

The particle measurement system consisted of a Nano-DMA (TSI Model 3085) and a UCPC (TSI Model 3025A). The diluted soot first passes through a radioactive ionizing source ( $\text{Po}^{210}$ ) which is installed prior to the Nano-DMA. An equilibrium charge distribution develops as the particles flow through the neutralizer with  $P(D_p)$ , the probability that a particle with diameter  $D_p$  carries one elementary unit of charge. The charge distribution obtained is in good agreement with the Boltzmann charge distribution [10]. In the size range examined in this study, the Boltzmann equilibrium contains only small fractions of +1 and -1 particles, nominally  $\approx 1\%$  at 3 nm and  $\approx 17\%$  at 50 nm. Wiedensohler [11] has developed an approximation of the bipolar charge distribution.

The positively charged aerosol particles enter at the outer annular tube of the DMA and moves toward the central rod under the influence of the electric field. A small flow of particles exit through a slit in the central rod of the DMA and are counted by a UCPC. The number concentration of particles exiting from the DMA,  $N(V)$ , at voltage  $V$ , is related to the integral of the product of the DMA transfer function,  $\Omega$ , and the size distribution function  $G(D_p) = dN/dD_p$ , where  $G(D_p)dD_p$  is equal to the number of particles per  $\text{cm}^3$  with diameter between  $D_p$  and  $D_p + dD_p$ :

$$N(V) = \int_0^\infty \Omega(Z_p, V) \cdot G(D_p) \cdot P(D_p) \cdot \left| \frac{dD_p}{dZ_p} \right| dZ_p \quad (1)$$

This explicit form of the equation was derived by Mulholland et al. [12]. The transfer function  $\Omega$  for the DMA operating at voltage  $V$  is defined as the probability that a charged particle entering the DMA with electric mobility  $Z_p$  will leave through the sampling slit. The transfer function was assumed to have a triangular shape with a peak

value of 1, and for a perfectly monodisperse aerosol, all the aerosol entering the DMA exits through the slit in the center electrode. The electric mobility corresponding to the peak in the transfer function for a voltage is given by the following equation:

$$Z_p = \frac{Q_c}{2\pi VL} \ln(r_2/r_1) \quad (2)$$

where  $Q_c$  is the flow of the sheath gas (10 SLPM),  $r_1$  and  $r_2$  are the inner and outer diameters of the classifying region, and  $L$  is the length of the classifying region. This equation is valid provided the sheath air flow is equal to the excess flow,  $Q_m$ , leaving the classifier.

In general, an expression for the electric mobility of a singly charged particle involving the particle diameter is obtained by equating the electric field force with the Stokes drag force:

$$Z_p = \frac{eC_c(D_p)}{3\pi\mu D_p} \quad (3)$$

where  $\mu$  is the air viscosity,  $e$  is the electron charge, and  $C_c(D_p)$ , the Cunningham slip correction factor, which corrects for the non-continuum gas behavior on the motion of small particles.

The concentration of the monodisperse aerosol leaving the Nano-DMA is monitored using the UCPC. The number concentration is measured as a function of voltage as the voltage is stepped up from about 10 to 5000 V, corresponding to particle diameters of approximately 3–60 nm, using 30 bins. A typical experiment consisted of setting the voltage constant for 10 s and recording number concentration data from the UCPC for 5 s (1 sample per second) at each bin. Initially a rapid scanning procedure was used, but there were problems with lack of repeatability between the upward and downward scans. The number concentration reported by the UCPC, the CO concentrations of the diluter and PFR section, and voltage was recorded with using a custom data analysis program.

In general, the determination of the size distribution requires the inversion of Eq. (1). For the case where the size distribution is broad and changing slowly with diameter in comparison with the transfer function, an approximate expression can be obtained for the size distribution function:

$$\frac{dN}{d \log(D_p)} = \frac{Q_c \left[ 2C_c(D_p) - 1 + \gamma\beta e^{(-\frac{D_p}{2\lambda})} \right] N_{\text{cpc}} \eta_{\text{para}} \eta_{\text{dil}}}{Q_a C_c(D_p) P(D_p) \eta_{\text{cpc}} \eta_{\text{loss}}} \quad (4)$$

where  $N_{\text{cpc}}$  is the output of the condensation particle counter,  $\lambda$  is the mean free path in air, and  $\alpha$ ,  $\beta$ ,  $\gamma$ , are constants taken from Kim et al. [13]. Several correction factors are applied to correct the UCPC measurement for probe dilution ratio,  $\eta_{\text{dil}}$ , diffusion losses during transport,  $\eta_{\text{loss}}$ , UCPC

detection efficiency,  $\eta_{\text{epc}}$ , and coincidence effects,  $\eta_{\text{para}}$  [14]. The diffusion losses were estimated through the two transfer lines using the procedure of Zhao et al. [8] for the turbulent section and that of Hinds [15] for the laminar section. The transfer efficiency through the turbulent section was defined as:

$$\eta_{\text{turbulent}} = e^{-\frac{D(D_p)\sigma_s}{\delta}\tau} \quad (5)$$

where  $D$  is the diffusion coefficient,  $\sigma_s$  is the surface to volume ratio,  $\tau$  is the transfer time, and  $\delta$  is the thickness of the laminar sublayer. The laminar sublayer thickness was estimated based on a smooth pipe [16] and the diffusion coefficient was obtained from Hinds [15]. The transfer efficiency throughout the turbulent section ranged from 0.47 at 3 nm to 0.94 at 10 nm and approached unity at larger particles sizes. The transfer efficiency through the laminar section was defined as [17]:

$$\eta_{\text{laminar}} = 0.819e^{-3.657\mu} + 0.097e^{-22.3\mu} + 0.032e^{-57\mu} \quad (6)$$

where  $\mu$  is the deposition parameter ( $\mu = DL/Q$  where  $D$  is the diffusion coefficient of the particles,  $L$  the length of tube, and  $Q$  the volume rate of flow through the tube) through the laminar section, the transfer efficiency ranged from 0.70 at 3 nm to 0.91 at 10 nm and approached 0.95 at larger particles sizes. The multiplication of the two efficiencies was used to determine the total transfer efficiency,  $\eta_{\text{loss}}$ . An uncertainty analysis was performed to define the expanded uncertainty (95% confidence level) for the particle diameters and particle concentrations [18]. Based on this analysis, the expanded uncertainty in the reported particle diameter was  $\pm 5\%$  and  $\pm 22\%$  in the reported concentration. The two main sources of uncertainty in the particle diameter resulted from voltage and Cunningham slip correction factor, while the main sources for the particle concentration resulted from the UCPC measurement uncertainty and particle loss estimations.

A rapid insertion probe was fabricated to thermophoretically collect particles from the reactor for transmission electron microscopy (TEM) imaging. The 3 mm diameter TEM grid was held in place by a miniature fork-shaped assembly contacting the TEM grid at its periphery. The pneumatically driven device collected soot for 0.5 s. The collected samples were imaged using a JEOL 1200 TEM.

Gas samples were analyzed by gas chromatography to quantitatively determine the concentration of the major intermediate species. The gas sampling system consists of four components: the sample probe, particle filtration and sampling, sample collection and retention, and the gas chromatograph. The gas sample collection system was heated to 200 °C to prevent condensation of

heavier hydrocarbon species. An Agilent 6890N gas chromatograph was used to quantitatively analyze the gas samples. Separation of gaseous species was achieved using a HP GasPro PLOT column (to measure light gases up to naphthalene). Quantification of gas concentrations was obtained using a flame ionization detector (FID). Peak identification and detector responsiveness are determined using calibrated gas standards.

### 3. Results

For the present experiments, ethylene was used as the fuel. The air flow rate was kept constant at 175 SLPM and the ethylene fuel flow rate was varied near the soot inception point. Under these flow conditions, the residence time in the WSR was on the order of 11 ms. Data was collected at four equivalence ratios near the soot inception point, namely  $\Phi = 1.8, 1.9, 2.0,$  and  $2.1$ . The expanded uncertainty in the reported equivalence ratios was  $\pm 3\%$ . The two main sources of uncertainty in the equivalence ratio resulted from the calibration uncertainty of the fuel and repeatability in the calibrations.

The soot size distribution results are plotted in Fig. 2 for four values of the equivalence ratio. For reasons discussed below, all soot size distributions reported in Fig. 2 were obtained at a nominal dilution ratio of 1000. The CO measurement technique enabled dilution measurements with an expanded uncertainty of  $\pm 9\%$ . Lognormal fits were applied to the particle size distributions. As can be seen in Fig. 2, the particle size distribution

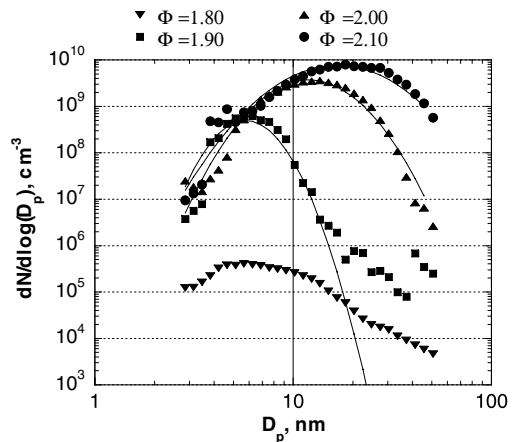


Fig. 2. Soot size distributions obtained with the NanoDMA are plotted for the WSR operating at four equivalence ratios close to the point of soot inception. At  $\Phi = 1.8$ , there was no indication of flame generated particles. Lognormal fits are applied to the distributions.

data is well-represented by the lognormal fits. At  $\Phi = 1.8$ , there was no indication of flame generated particles. The actual particle concentration obtained by the UCPC for this condition was less than 1 particle  $\text{cm}^{-3}$  and the nominal value of  $10^5 \text{cm}^{-3}$  for the size distribution function was primarily a result of the 1000-fold dilution and the low charging probability of nanometer size particles. The peak in the size distribution at  $\Phi = 1.9$  was a couple orders of magnitude larger than the background, but also a couple of orders of magnitude less than the values observed at the higher equivalence ratios. The peak in the size distribution at  $\Phi = 1.9$  occurred at a particle size of 5–8 nm compared to 15–16 nm for  $\Phi = 2.0$ , and a broad peak extending from about 15–22 nm for  $\Phi = 2.1$ . The size distribution at  $\Phi = 2.1$  was significantly broader than the other two. These results demonstrate that soot size distributions obtained using our WSR/PFR were sensitive to equivalence ratio.

Soot size distribution measurements were made as a function of dilution ratio. As demonstrated in Fig. 3, the soot size distributions were not affected by the increased dilution. A critical dilution ratio on the order of 1000 was necessary to mitigate coagulation growth in the sampling line [5]. If coagulation were taking place during the dilution process, the size distribution of the more concentrated soot would be shifted to larger particle sizes. This behavior was observed as the dilution ratio was stepped down, from 1000, at a fixed equivalence ratio.

Figure 4 displays the influence of temperature on the measured soot size distributions in the PFR. Temperature measurements were made in the WSR section by two type-B thermocouples of differing bead sizes, 0.81, and 1.08 mm. Due

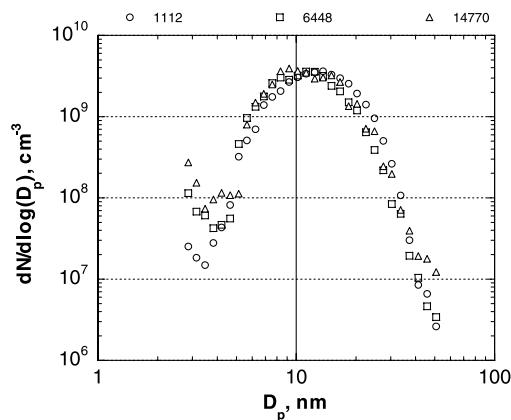


Fig. 3. The effect of the dilution ratio on the measured soot size distribution. Experimental conditions: equivalence ratio,  $\Phi = 2.0$ , dilution ratio varied from 1112 to 14770.

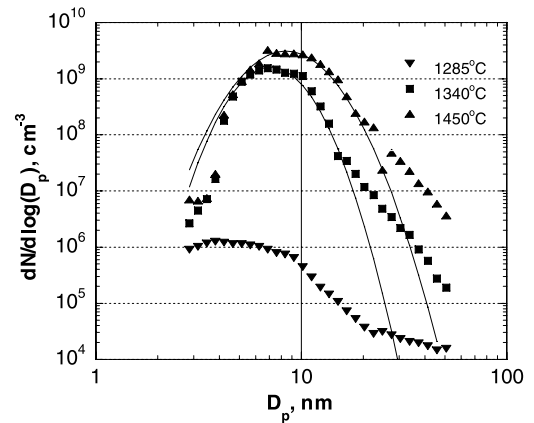


Fig. 4. The effect of temperature on the measured soot size distribution. Experimental conditions: dilution ratio 1000, equivalence ratio,  $\Phi = 2.0$ . Lognormal fits are applied to the distributions.

to the very high velocity field in the WSR section, convective heat transfer to the thermocouples dominates the radiative losses to the walls of the WSR. Consequently, the temperatures reported for the WSR have not been corrected for radiative losses. Temperature measurements in the PFR section had to be corrected for radiative losses due the significantly slower velocity field. Three type-B thermocouples of differing bead sizes, 0.38, 0.78, and 1.07 mm, were used to estimate the gas temperature. Each bead was corrected for radiative losses, assuming spherical beads. Iteration of the energy balance of the beads was used to determine the wall temperature, emissivity, and gas temperature. Under sooting conditions ( $\Phi = 2.0$ ), the procedure is complicated by the possibility of soot accumulation on the beads. The effects of the accumulation were estimated by varying the emissivity and bead sizes. Using reasonable changes in these properties only increased the calculated gas temperature by less than 50 °C. Based on this analysis, the expanded uncertainty in the temperature measurements was  $\pm 10\%$ .

The temperature of the WSR section was altered by adjusting the flow of nitrogen, from 0 SLPM to 30 SLPM. All of the soot size distributions reported in Fig. 4 were obtained at a fixed equivalence ratio of  $\Phi = 2.0$ . From the figure, an addition of 20 SLPM of nitrogen resulted in a decrease of the measured WSR from 1450 to 1340 °C. Under these conditions, the soot size distributions measured in the PFR section did not change significantly. Specifically, the peak particle size was reduced from 10 to about 8 nm. When the nitrogen flow was increased to 30 SLPM in the WSR section, the temperature measured in the WSR section decreased to 1285 °C (from 1450 °C under 0 SLPM nitrogen flow). Soot

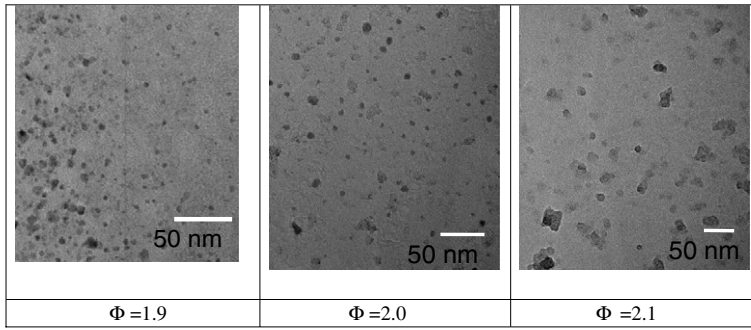


Fig. 5. Images obtained from transmission electron microscope of soot samples collected from the PFR at three different equivalence ratios.

particles were no longer detected within the PFR section under these conditions. The effects of temperature and dilution on soot inception have been well-characterized for other flames. A critical temperature for soot inception in diffusion flames has been observed to occur around 1375 °C [1]. From our results, at  $\Phi = 2.0$ , it was observed that soot formation was suspended when the WSR section was reduced to 1285 °C.

It was desired to view the particles characterized by the Nano-DMA/UCPC using an independent method. As a result, the particles were sampled using the rapid insertion probe at the same height as the dilution probe. Multiple insertions were required to obtain a high enough particle density to image the particles using the TEM. Fig. 5 displays characteristic images for particles collected at  $\Phi = 1.9, 2.0$ , and 2.1. It is important to note that the higher magnifications were required to images particles at  $\Phi = 1.9$  as compared to  $\Phi = 2.0$  and 2.1. The soot particles observed under the TEM were droplet-like at the soot inception point,  $\Phi = 1.9$ . These observations of soot particle morphology agree qualitatively with the soot inception study of Dobbins et al. [19]. It is important to note that no particles were observed under the TEM at  $\Phi = 1.8$ .

#### 4. Discussion

The soot size distributions obtained from our WSR/PFR were sensitive to equivalence ratio. During particle growth, the particle size distribution changes as a function of time. For coagulation in the continuum regime, the self-preserving distribution (SPD) was obtained for the first time by Friedlander and Wang [20] using a similarity transform to the size distribution function, which is independent of the initial conditions. Subsequently, it was shown that the SPD was also valid in the free molecular regime. Vemury and Pratsinis [21] studied the self-preserving distributions in the free-molecular and continuum regimes for

agglomerates of various fractal dimensions using their coagulation model. The similarity solutions of Vemury and Pratsinis [21] have been applied to a wide variety of problems including the calculation of SPD for coagulation in sooting flames [22].

Self-preserving size distributions corresponding to the particle size distributions measured at  $\Phi = 1.9, 2.0$ , and 2.1 were calculated by applying the similarity solutions of Vemury and Pratsinis [21]. Fig. 6 shows the soot particle size distribution for equivalence ratios  $\Phi = 1.9, 2.0$ , and 2.1 with the calculated SPD's. The width of the log-normal distribution for  $\Phi = 1.9$  is  $\sigma_g = 1.31$  and this value increases to  $\sigma_g = 1.48$  for  $\Phi = 2.0$ , and  $\sigma_g = 1.65$  for  $\Phi = 2.1$ . Vemury et al. [23] computed  $\sigma_g = 1.46$  for SPD in the free molecular regime. The particle size distribution obtained at  $\Phi = 2.0$  was closest to the SPD for coagulation in the free molecular regime. In the present experiments,  $\Phi = 1.9$  was observed to be the soot inception point for the WSR/PFR. Particle coagulation is not expected to be the dominant mechanism of

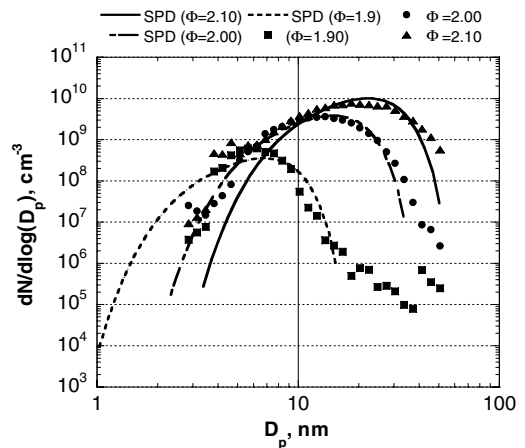


Fig. 6. Comparison to self preserving size distribution at free molecular regime for three equivalence ratios.

Table 1

The results of species quantified using gas chromatography (GC) measurements for key species thought to be important in soot formation and growth

Species	Equivalence ratio		
	1.85	2.0	2.2
Acetylene	8700	11,800	16,000
Benzene	17	35	210
Indene	0.4	1.0	5
Naphthalene	0.6	1.8	20

All values must be multiplied by  $1 \times 10^{-6}$ .

particle growth at particle inception. Therefore, the width of the lognormal distribution was expected to be smaller than the SPD at  $\Phi = 1.9$ .

It is crucial to compare the soot size distribution obtained in a WSR/PFR to those measured in laminar flames. As mentioned, particle size distributions measured in a WSR/PFR are expected to be closer to those in actual combustors. Maricq et al. [9,22] and Zhao et al. [8,24] reported size distribution measurements for soot collected from a pre-mixed ethylene-air flame generated by a 6 cm diameter, water cooled, McKenna burner. The authors used a Nano-DMA similar to the one here and a high dilution probe, also similar to the one reported presently. The size distribution obtained by Maricq et al. [9,22] for  $\Phi = 2.06$  had a peak at the smallest size measured, independent of the sampling height. This was qualitatively different from our findings. The reason for the difference may be the different combustion environment for a WSR compared to a premixed burner. In the WSR, the incoming fuel and air are rapidly mixed with the products of combustion including incipient soot, CO, PAHs, and free radicals; whereas, in a premixed burner, the combustion products are not back mixed into the fuel and air. The difference in mixing may also affect the size distribution. The soot inception region may terminate within the WSR so that only particle growth is occurring in the PFR section where the particles were sampled. The very low particle number concentrations observed at  $\Phi = 1.9$  might be a result of the WSR/PFR being operated so close to the soot inception point.

To qualitatively explore the relationship between light gas species concentrations and particulate formation, gas chromatography was performed on samples obtained from the WSR/PFR at the same operating conditions used for particle measurements at  $\Phi = 1.85$  and 2.0. To extend the analysis to heavily sooting conditions, additional measurements were made at  $\Phi = 2.2$ . All concentrations are on a mole basis (see Table 1). Expanded uncertainties in concentrations are approximately  $\pm 5\%$  for acet-

ylene and  $\pm 15\%$  for the remaining species. At the non-sooting equivalence ratio of  $\Phi = 1.85$ , the concentration of benzene is low and that of larger aromatic species is less than  $1 \times 10^{-6}$ . At moderately sooting conditions, both benzene concentration and aromatic concentrations increase markedly (from a factor of 2 for benzene to a factor of 3 for naphthalene). At the highest studied equivalence ratio, the benzene and aromatic concentrations again increase by large amounts (3–5 times that at  $\Phi = 2.0$ ). Additionally, over the range of equivalence ratios studied acetylene concentrations approximately double. The results are consistent with the common understanding the acetylene and small aromatics are key species on the pathway to particulate formation and the qualitative trends in aromatic concentration are in good agreement with the changes in soot concentration observed using the Nano-DMA.

## 5. Conclusions

These results demonstrate that soot size distributions obtained using a WSR/PFR were sensitive to equivalence ratio. Furthermore, the present findings have demonstrated the ability to measure highly diluted particle size distributions using a gas-cooled dilution probe in a combustion environment with temperatures of  $\approx 1400$  K. The particle size distribution obtained at  $\Phi = 2.0$  was closest to the SPD for coagulation in the free molecular regime. A nucleation peak at the smallest particle size measured was observed with the premixed burner but not with the WSR.

## Acknowledgments

This work was supported by a grant to Drs. Manzello and Tsang through the Strategic Environmental Research and Development Program (SERDP). Mr. Charles Pellerin is the program manager. The assistance of Mr. Marco G. Fernandez of BRFL-NIST with the experimental setup was crucial in performing the experiments.

## References

- [1] I. Glassman, *Proc. Comb. Inst* 22 (1988) 295–311.
- [2] H. Richter, J.B. Howard, *Proc. Eng. Combust. Sci.* 26 (2000) 565–608.
- [3] F.W. Lam, J.P. Longwell, J.B. Howard, *Proc. Comb. Inst.* 22 (1988) 323–332.
- [4] L.G. Blevins, K.A. Jensen, R.A. Ristau, N.Y.C. Yang, C.W. Frayne, R.C. Striebich, M.J. DeWitt, S.D. Stouffer, E.J. Lee, R.A. Fletcher, J.M. Oran, J.M. Conny, G.W. Mulholland, *Soot Inception in a Well Stirred Reactor*, 3rd Joint Meeting of the US

- Sections of the Combustion Institute, Chicago, Illinois, March 2003.
- [5] S.L. Manzello, G.W. Mulholland, M.T. Donovan, K. Park, M.R. Zachariah, S. Stouffer, *On the use of a well stirred reactor to study soot inception*, 4th Joint Meeting of the US Sections of the Combustion Institute, Philadelphia, PA, March 2005.
- [6] J.P. Longwell, M.A. Weiss, *Ind. Eng. Chem.* 47 (1955) 1634–1642.
- [7] S.D. Stouffer, R.C. Striebich, C.W. Frayne, J. Zelina, *Combustion Particulates Mitigation Investigation Using a Well-Stirred Reactor*, 38th Joint Propulsion Conference and Exhibit, 7–10 July 2002 Indianapolis, Indiana, AIAA 2002-37.
- [8] B. Zhao, Z. Yang, J. Wang, M.V. Johnston, H. Wang, *Aerosol Sci. Tech.* 37 (2003) 611–620.
- [9] M.M. Maricq, *Combust. Flame* 37 (2004) 340–350.
- [10] S.H. Kim, B.Y.H. Liu, M.R. Zachariah, *J. Coll. Interface Sci.* 282 (2005) 46–57.
- [11] A. Wiedensohler, *J. Aerosol Sci.* 19 (1988) 289–387.
- [12] G.W. Mulholland, M.K. Donnelly, C. Hagwood, S.R. Kukuck, R. Hackley, D.Y.H. Pui, *J. Res. NIST*, in press (2006).
- [13] J.H. Kim, G.W. Mulholland, S.R. Kukuck, D.Y.H. Pui, *J. Res. NIST* 110 (2005) 31–54.

- [14] J. Kesten, A. Reinking, *Porstendorfer, Aerosol Sci. Technol.* 15 (2005) 107–111.
- [15] W.C. Hinds, *Aerosol Technology: Properties, Behavior, and Measurement of Airborne Particles*, 483, John Wiley and Sons, New York, 1998.
- [16] R.P. Benedict, *Fundamentals of Pipe Flow*, 531, John Wiley and Sons, New York, 1980.
- [17] S.K. Friedlander, *Smoke, Dust, and Haze: Fundamentals of Aerosol Dynamics*, 432, Oxford University Press, New York, 2000.
- [18] B.N. Taylor, C.E. Kuyatt, *Guidelines for Evaluating and Expressing the Uncertainty of NIST Measurement Results*, NIST TN 1297, September 1994.
- [19] R.A. Dobbins, R.A. Fletcher, H.C. Chang, *Combust. Flame* 115 (1998) 285–298.
- [20] S.K. Friedlander, C.S. Wang, *J. Coll. Interface Sci.* 22 (1966) 126–135.
- [21] S. Vemury, S.E. Pratsinis, *J. Aerosol Science* 26 (1995) 175–185.
- [22] M.M. Maricq, S.J. Harris, J.J. Szente, *Combust. Flame* 132 (2003) 324–328.
- [23] S. Vemury, K.A. Kusters, S.E. Pratsinis, *J. Coll. Interface Sci.* 165 (1994) 53–59.
- [24] B. Zhao, Z. Yang, M.V. Johnston, H. Wang, A. Wexler, M. Balthasar, M. Kraft, *Combust. Flame* 133 (2003) 173–188.

## Comments

*Alessandro Gomez, Yale University, USA.* The uncertainty that you mentioned on particle size and concentration would be very desirable for measurements in flames aimed at determining the structure of the sooty region. In well-stirred reactors, spatial resolution is not an issue, unlike flame environments. Can you elaborate on the feasibility of miniaturizing your probe for possible applications in diffusion flames? Could it ever reach quartz microprobe size with micro-fabrication techniques, or are dilution requirements too severe?

*Reply.* For diffusion flame applications, it would be desirable to reduce the size of the sampling probe. An important consideration for such probes is that sufficient dilution is available in order to minimize coagulation growth in the sampling line. In our measurements using the well stirred reactor/plug flow reactor, a critical dilution ratio on the order of  $10^3$  was necessary to mitigate coagulation growth. Similarly, high dilution ratios are also necessary to minimize coagulation growth in the sampling line for other premixed flame systems [1,2]. Although we have not attempted to fabricate a smaller sized probe, similar in size to a quartz microprobe, from a hydrodynamic perspective, it indeed may be possible to fabricate such a probe to yield sufficient dilution requirements. However, clogging of the microprobe tip and how rapidly the dilution was applied after the microprobe tip to avoid coagulation growth would be of critical importance. This would be an interesting area for further research.

## References

- [1] B. Zhao, Z. Yang, M.V. Johnston, H. Wang, A. Wexler, M. Balthasar, M. Kraft, *Combust. Flame* 133 (2003) 173–188.
- [2] M.M. Maricq, S.J. Harris, J.J. Szente, *Combust. Flame* 132 (2003) 324–328.



*William Green, MIT, USA.* Your data suggests that your measurements for the smallest particles are sensitive to the dilution rate and that you might actually be seeing one hump of a bimodal distribution. How do you know that your gas does not contain a large number of 1 nm particles?

*Reply.* The ultrafine condensation particle counter (UCPC) used during this experimental study is limited to measuring particles that have sizes greater than 3 nm, making direct measurement of 1 nm particles not possible at this time using the UCPC. To address this issue, we designed a rapid insertion probe to collect particles and then imaged these particles using a transmission electron microscope (TEM). Based upon a preliminary analysis of the particle sizes imaged using the TEM, we did not observe particles smaller than 2 nm at the bottommost port of our PFR, the location at which all data is reported in this study.

Finally, a wide range of dilution rates were investigated to elucidate the effects of sampling dilution ratio on the measured size distribution of the particles. At

low dilution ratios (below  $10^3$ ), an appreciable shift in the peak particle size in the particle size distribution was observed. Once above this critical dilution ratio, no shift was observed, even with dilution ratios up to  $10^4$ . Zhao et al. [1] used similar dilution ratios and a similar probe design to achieve sufficient quenching to limit coagulation and to measure an inception peak in laminar flames. Measurements have been made to ensure that the inception peak can be measured in our WSR/PFR facility by operating under conditions which only an inception peak is present and the most abundant

diameter was observed at the lower limit of the UCPC detection capability. These factors suggest that the reason why no inception peak was measured at the bottom-most port of the PFR section of our WSR/PFR facility is a result of the mixing properties of the WSR, not a sampling artifact.

### Reference

- [1] B. Zhao, Z. Yang, J. Wang, M.V. Johnston, H. Wang, *Aerosol Sci. Tech.* 37 (2003) 611–620.